Going in the right direction

Cellular mechanisms underlying root halotropism

Korver, R.A.

Publication date
2019

Document Version
Other version

License
Other

Chapter 2:

Out of Shape During Stress: A Key Role for Auxin *

Ruud A. Korver[1], Iko T. Koevoets[2], and Christa Testerink [2]

[1]University of Amsterdam, Plant Cell Biology, Swammerdam Institute for Life Sciences, 1090GE Amsterdam, The Netherlands
[2]Laboratory of Plant Physiology, 6708PB Wageningen University and Research, Wageningen, The Netherlands

*Published in Trends in Plant Sciences, June 2018 doi: 10.1016/j.tplants.2018.05.011

Abstract:
In most abiotic stress conditions, including salinity and water deficit, the developmental plasticity of the plant root is regulated by the phytohormone auxin. Changes in auxin concentration are often attributed to changes in shoot-derived long-distance auxin flow. However, recent evidence suggests important contributions by short-distance auxin transport from local storage and local auxin biosynthesis, conjugation, and oxidation during abiotic stress. We discuss here current knowledge on long-distance auxin transport in stress responses, and subsequently debate how short-distance auxin transport and indole-3-acetic acid (IAA) metabolism play a role in influencing eventual auxin accumulation and signaling patterns. Our analysis stresses the importance of considering all these components together and highlights the use of mathematical modeling for predictions of plant physiological responses.

Auxin on the Move During Stress

Drought and increasing salinity are abiotic stresses that cause major decreases in crop yield worldwide. Drought causes loss of crops through water deficit, whereas increasing soil salinity induces osmotic and ionic stress in the plants. Both abiotic stresses are a threat to the amount of arable land that is fit for our food production. Although the development of crops tolerant to these conditions has received attention [1], a greater research focus has been on generating biotic stress resistance and increasing the yield of edible parts of the plant. Now that we face a rapid deterioration of arable land, research on the tolerance to abiotic stresses has substantially increased. Phenotypic plasticity, including developmental modifications to root system architecture (RSA), is vital for tolerance to water deficiency and high soil salinity.

RSA and root growth rates during plant development under optimal conditions have been well studied, and it has long been established that these require the phytohormone auxin. Recently our fundamental understanding of root developmental plasticity during abiotic stress has markedly improved [2]. Unsurprisingly, auxin plays an important role during abiotic stress-induced changes in the root. Through the creation of local auxin maxima, cell elongation is locally inhibited and the emergence of lateral roots can be arrested. On the other hand, local auxin minima were found to be a signal that triggers the transition from cell division to cell differentiation in roots of arabidopsis (Arabidopsis thaliana) [3]. The different processes that together determine auxin-mediated regulation of growth and development during abiotic stress are auxin transport, biosynthesis, conjugation, perception, and signaling. Auxin transport has received much attention, and the role of polar auxin transport

(PAT) by auxin carrier proteins during unstressed conditions and gravitropism has been well established [4–6]. By contrast, the changes in PAT during abiotic stresses remain largely unknown. How changes in local auxin biosynthesis and IAA conjugation during abiotic stress affect root responses is another relatively young field of research. The integration of all these different aspects of auxin homeostasis is complicated because the many factors involved all influence each other and there is extensive crosstalk between auxin and other hormones. One promising solution to this problem is the rapidly emerging field of computational modeling of auxin processes in the plant root.

Auxin Transport from Shoot to Root

The main mechanism to maintain the 'upside-down fountain' of auxin flow in the root is PAT. Clarification of the role of long-distance shoot-derived auxin transport in abiotic stress has advanced our understanding of the changes in auxin carrier proteins and other proteins that influence auxin flow in the root (Figure 1). Internalization of the auxin efflux carrier PIN-formed 2 (PIN2) either during halotropism on the side of the root facing a higher salt concentration [7] or during osmotic stress treatments [8] has been shown. Subsequently, by combining *in planta* salt stress experiments with computational modeling, it was concluded that internalization of PIN2 is not sufficient to explain the alteration of auxin flow during halotropism [9], and changes in PIN-formed 1 (PIN1) and auxin transporter protein 1 (AUX1) were shown to co-facilitate the fast change of auxin flow. In addition to root growth, auxin efflux carriers are suggested to regulate meristem size during salt stress [10]. Reduced PIN1, PIN3, and PIN7 expression and auxin-resistant 3 (AXR3)/indole-3-acetic acid 17 (IAA17) stabilization during salt stress have been proposed to influence the root meristem size by increasing nitric oxide (NO) levels.

Another large family of auxin carriers influencing auxin flow in the root is the ABCB transporter family [11]. Recently, several studies have shown a role for ABCB transporters during salt stress. Of 22 different ABCB transporters in rice (*Oryza sativum*), the expression of 21 was found to change in response to salinity and drought [12,13]. Of the root-expressed ABCB auxin transporters, the expression of ABCB1 and 19 was slightly upregulated, whereas ABCB4 showed downregulation after 1 h of salt stress. Reduced acropetal transport of auxin was observed in an *abcb19* null mutant, whereas basipetal transport was unaltered [14].

Other genes, whose loss-of-function mutants were recently observed to exhibit altered auxin flow in the root, are putatively involved in abiotic stress tolerance. Mutants of interactor of synaptotagmin 1 (ROSY1-1) showed a

decrease in basipetal auxin transport and exhibited increased salt tolerance, which was ascribed to the interaction between ROSY1-1 and synaptotagmin 1 (SYT1) [15]. Furthermore, zinc-induced facilitator-like 1 (ZIFL1), a major facilitator superfamily (MFS) transporter, regulates shootward auxin efflux in the root [16]. *zifl1* loss-of-function mutants were observed to have reduced PIN2 protein abundance in epidermal root cells after external application of IAA and had gravitropic bending defects.

Auxin Transport from Close By

Changes in auxin transport between different intracellular compartments also influence the auxin that is available for the formation of local auxin maxima. Auxin located in the acidic vacuole, with a pH of 5.0 to 5.5, will tend to move towards the cytosol which has a pH of 7. During salt stress the cytosolic pH drops [17], thus theoretically reducing passive auxin efflux from the vacuole. Apoplastic pH is also suggested to be involved in passive auxin influx into the cells (Box 1).

Isolated vacuoles from protoplasts lacking the tonoplast-located auxin carrier WAT1 (walls are thin 1) were found to accumulate significantly more radiolabeled auxin than wild-type vacuoles, indicating active transport of auxin from the vacuole to the cytoplasm by WAT1 [18]. Recently, an auxin transport facilitator family, located on the endoplasmic reticulum (ER), was identified. PIN- LIKES (PILS) proteins are believed to be involved in auxin homeostasis through auxin accumulation at the ER, in this way limiting the IAA available for nuclear auxin signaling. The change in available IAA alters the cellular sensitivity to auxin. Increased auxin export from *pils2/pils5* protoplast cells was also observed [19]. In addition, a *pils2* arabidopsis mutant, and even more so a *pils2/pils5* double mutant, showed significantly longer roots than the wild type and a higher lateral root density, suggesting PILS involvement in auxin-dependent root growth. Other forms of passive auxin transport include movement without the interference of membranes. IAA is a small molecule and is therefore able to move freely through the plasmodesmata (PD) in its ionized form (IAA-). To restrict free cell-to-cell movement of IAA during auxin gradient formation, GLUCAN SYNTHASE-LIKE 8 (GSL8) induces an increase of plasmodesma-localized callose. This reduces the symplasmic permeability to maintain local auxin maxima [20]. GSL8 expression was found to be upregulated by adding exogenous IAA. Although these results demonstrate the importance of local auxin movement, the relation to abiotic stress remains to be elucidated.

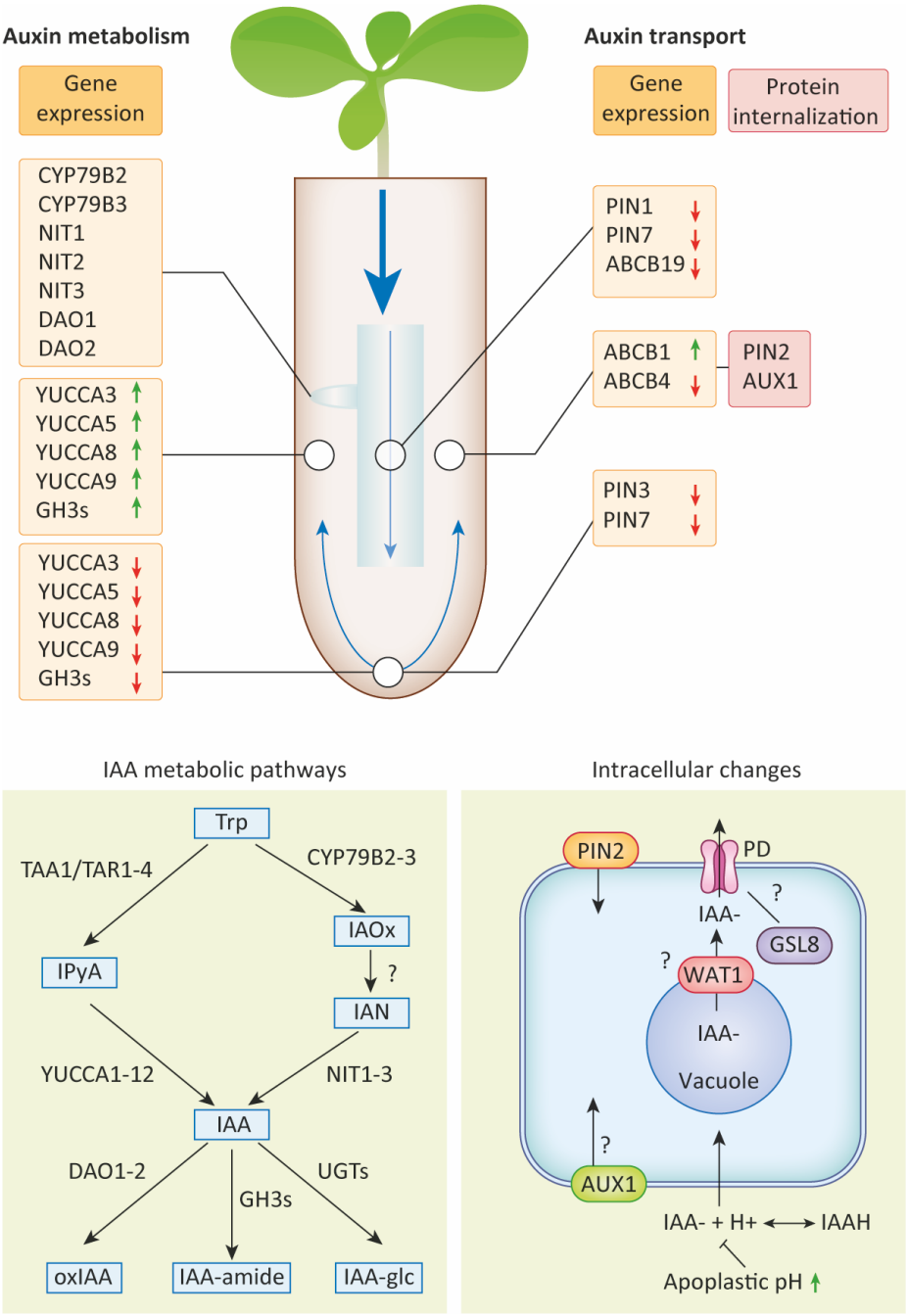

Figure 1. Schematic Overview of Salt Stress-Induced Changes in Auxin Biosynthesis, Conjugation, and Transport-Related Processes in the Arabidopsis Roots. (A) Indole-3-acetic acid (IAA) metabolism. The level of IAA is tightly regulated by IAA biosynthesis, conjugation, and degradation, together determining the IAA status of a cell. The lower panel shows part of the known IAA biosynthesis ([21,22] for a complete overview) and conjugation (continued below)

Controlling the Levels of Auxin

In addition to transport, auxin (IAA) levels are determined by biosynthesis and conjugation. Both processes have recently shown to be affected by abiotic stress in the root.

Although several IAA biosynthesis pathways has been described [21,22], the indole-3-pyruvic acid (IPyA) pathway is considered to be responsible for most IAA biosynthesis in higher plants [23,24]. In addition, for the Brassicaceae family, the indole-3-acetaldoxime (IAOx) pathway has been increasingly identified to play a role during several stress responses [25–27], whereas the significance of the other pathways remains under debate and needs further research [21,22]. We focus here on the IPyA and IAOx pathways, and on how these pathways are modulated during abiotic stress.

The IPyA pathway (Figure 1) generates IAA via a two-step conversion from tryptophan, with IPyA as the intermediate [27–29]. The family of YUCCA proteins governs the second step of the pathway [27]. Eleven YUCCA isoforms have been described in arabidopsis, and specific roles for several YUCCAs are slowly being elucidated. The YUCCAs can be divided into mainly

Figure 1 continued: pathways and the known involved genes or gene families. Based on microarray data of two different studies (Table S1), we have identified gene expression patterns with promising possibilities for influencing eventual IAA accumulation patterns and signaling. For genes in the IAOx pathway we observe strong expression in zone 4 (Figure 2C), which is the zone containing primordia and lateral roots. All genes are also influenced by salt stress in a time-dependent matter (Table S1). We see a similar pattern for DAO1 and DAO2. Both DAO1 and CYP79B2-3 have been linked to lateral root development and show expression specifically underlying newly formed lateral roots. YUCCA 3, 5, 8, and 9, together with the GH3 family genes, show upregulation in the epidermis and cortex during salt stress, whereas they are downregulated in the columnella (Figure 2B). (B) Auxin transport. During salt stress, expression of the auxin efflux carriers PIN1, PIN7, and ABCB19 in the stele is downregulated. In the columnella, PIN3 and PIN7 are downregulated. In epidermal and cortical cells, PIN2 and ABCB4 auxin efflux carriers are downregulated whereas ABCB1 is slightly upregulated. In epidermal cells, on a cellular level, PIN2 is internalized and changes in AUX1 abundance at the plasma membrane during halotropism were observed, providing evidence that AUX1 is also internalized [9]. Putatively, the activity of the tonoplast-located WAT1 undergoes changes to alter intracellular auxin levels following a change in cytosolic pH. To create local auxin maxima, the passive flow of IAA _ molecules through the plasmodesmata (PD) might need to be blocked. This is putatively achieved through GSL8-mediated callose deposition. The apoplastic pH increase following salt exposure of the root potentially inhibits the passive influx of IAAH into the cell. Blue arrows depict auxin flow, grey boxes show up- (green arrow) or downregulation (red arrow) of genes during salt stress. Black boxes show plasma-membrane proteins that are internalized upon salt stress. Question marks show processes that influence local auxin concentrations but have not yet been proved to be involved in local auxin changes during abiotic stress. Abbreviations: IAA-, ionized IAA; IAA-glc, IAA-glucose; IAAH, protonated IAA; IAN, indole- 3-acetonitrile; IAOx, indole-3-acetaldoxime; IPyA, indole-3-pyruvic acid; oxIAA, oxidized IAA (2-oxindole-3-acetic acid); PD, plasmodesma; Trp, tryptophan.

root-or shoot-active proteins [30,31]. YUC3, 5, 7, 8, and 9 display distinct expression patterns in the root, whereas other YUCCAs show minor or no expression in the root [30]. This illustrates the specificity of different genes in this pathway for specific developmental processes. Although little research on the specificity of YUCCAs for different stresses has been carried out, several gene expression studies do indicate this specificity. For example, YUC2, 5, 8, and 9 show upregulation in plants experiencing shade [32], and knockout mutants of these quadruple YUCCA lack shade-induced hypocotyl elongation [33]. Several papers show that overexpression of the IPyA pathway leads to increased salt tolerance in several species [34–36]. For example, it was shown in cucumber that specific YUCCAs are expressed at high and low temperature and in response to salinity [36]. In salinity, CsYUC10b is strongly upregulated and CsYUC10a and CsYUC11 are strongly downregulated, whereas overexpression of CsYUC11 leads to higher salinity tolerance [36]. For arabidopsis, the role of specific YUCCAs during salt stress is so far unknown. Analysis of previously published microarray data [37,38] confirms the root specificity of YUC3, 5, 8, and 9 (Table S1 in the supplemental information online). Furthermore, tissue-specific microarray data indicate a shift from strong expression of YUCCAs in columnella under control conditions to strong expression in the epidermis and cortex during salt stress (Figures 1, 2A, and Table S1). Because expression of YUCCAs is low in the epidermis and cortex under control conditions, and thus auxin levels in these cells would mainly depend on transport, this is an interesting shift. Salt stress also has major effects on auxin transport, and therefore epidermal biosynthesis is likely to affect auxin distribution during stress and is expected to have consequences for growth responses in the root.

The IAOx pathway (Figure 1) is *Brassica*-specific and has mostly been described for its role in secondary metabolism, producing both indole glucosinolates and camalexin [27,39–41]. More recently, however, several papers have pointed out a possible involvement of this pathway in local IAA production, specifically under stress conditions [25–27,42]. Sugawara *et al.* showed that, when plants were fed ^{13}C6-labeled IAOx, 40% of the ^{13}C6 atoms was incorporated into IAA, confirming that IAA can be formed from IAOx [42]. In 2002 Zhao *et al.* showed that a *cyp79b2 cyp79b3* double-knockout mutant showed reduced growth and reduced IAA production specifically under higher temperatures [27]. Recently, the same mutant was observed to have decreased lateral root growth during salt stress [25]. Whereas the IPyA pathway is mainly active in the differentiation and elongation zone of the main (and lateral) root, genes in the IAOx pathway are, in addition to expression in the QC, strongly

expressed in cells underlying newly developing lateral roots and lateral root primordia [43]. In accordance, all genes described in this pathway show strong expression in the differentiation zone (Figure 2A,B and Table S1) and their expression during salt stress is strongly time-dependent (Table S1), suggesting a major role for this pathway in salt-regulated lateral root development in arabidopsis.

Levels of free IAA are tightly regulated by several conjugation and degradation processes (Figure 1) [44]. Although IAA itself is both the active and transported compound in plants, it has a very high turnover. *In planta*, the levels of IAA conjugates and catabolites correlated strongly with the levels of free IAA in both root and shoot, and high levels of conjugates and catabolites are present when high levels of free IAA occur [45,46]. Levels of IAA catabolites are in general higher than of free IAA [45]. The strict regulation of free IAA levels is nicely illustrated by analysis of mutants in specific conjugation pathways – reduced conjugation via one pathway often leads to increased conjugation via other pathways and only minor changes in free IAA levels [47].

Ester conjugation is mainly governed by several UDP-glucose transferases (UGTs). In Table S1 we have summarized the UGTs that are currently known to conjugate IAA, but this list is probably not complete. These enzymes respond differently to salt stress (Figure 2C and Table S1), which might point to specific roles for specific UGTs.

Enzymes of the GRETCHEN HAGEN 3 (GH3) family form amide conjugates of IAA [48]. All involved GH3s appear to be strongly expressed in roots and are upregulated upon salt stress (Figure 1C and Table S1). In addition, GH3.5/WES1 is induced by many abiotic and biotic stresses as well as by ABA treatment [49]. Interestingly, upregulation of GH3s upon salt stress seems to be specific to epidermis, comparable to upregulation of YUCCAs.

IAA oxidation is responsible for most IAA turnover and leads to degradation of the compound [50]. Plants contain 10–100-fold more oxIAA than IAA conjugates, showing that the oxidation pathway is very active [45]. Two DIOXYGENASE FOR AUXIN OXIDATION (DAO1 and DAO2) enzymes have been described to be responsible for the first step of oxidation [51,52]. DAO1 and 2 show strong expression in zone 4, similarly to genes in the IAOx pathway (Figure 2B and Table S1). Zhang *et al.* have shown that DAO1 is expressed in cells underlying newly developing lateral roots, and that the knockout has increased lateral root density [52], indicating a possible role for IAA oxidation in root responses to salt stress.

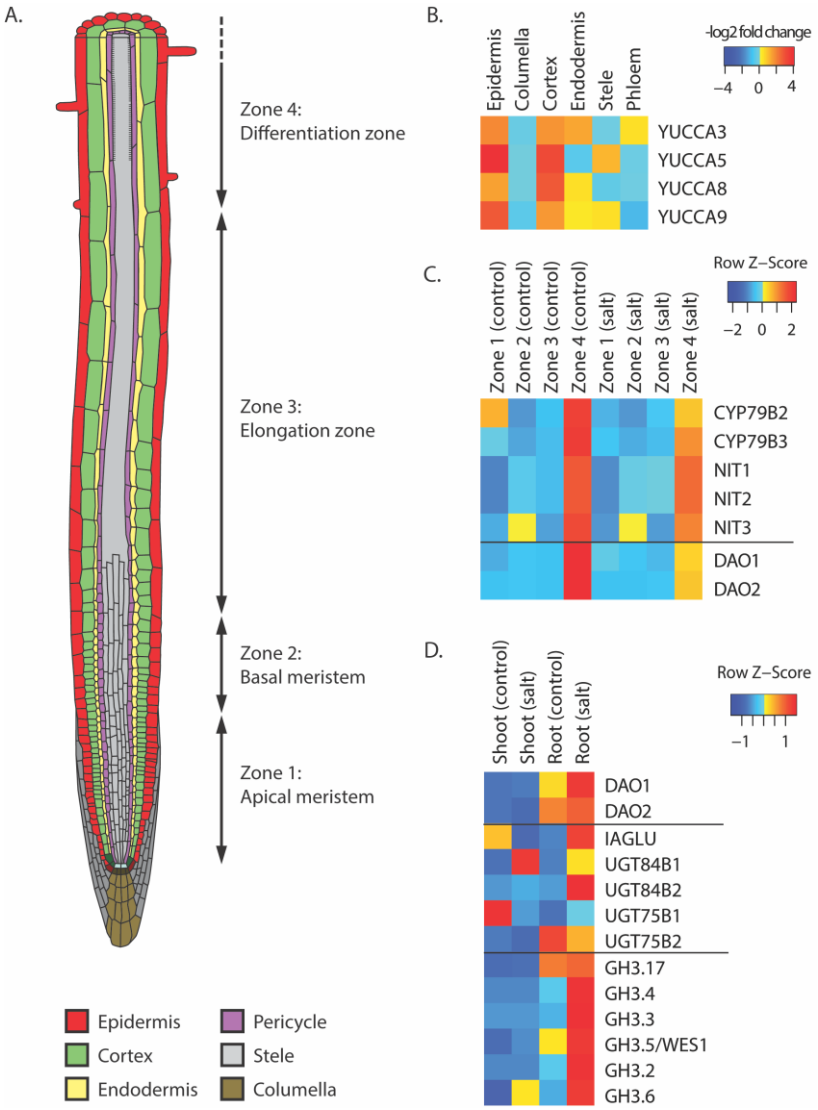

Figure 2. Illustration of Gene Expression of Auxin Homeostasis-Related Genes Showing Patterns That Could Be Relevant for Indole-3-Acetic acid (IAA) Accumulation Patterns in Abiotic Stress. (A) Heatmaps are based on microarray data of two different studies (Table S1). For tissue-specific and zone specific expression patterns, the root has been divided in different tissues and in four different root zones, as illustrated. Figure adapted, with permission, from Figshare (B. Peret, Primary and lateral root.ai; https://figshare.com/collections/Root_illustrations/3701038). (B) Heatmap of the relative expression (log_2 fold change) upon salt stress of YUC3, 5, 8, and 9 in different root tissues. (C) Heatmap of the expression of genes in the indole-3-acetaldoxime (IAOx) pathway and oxidation in different root zones under control conditions and during salt stress. The heatmap is normalized per gene. (D) Heatmap of the expression of genes involved in IAA conjugation in the shoot and root under control conditions and during salt stress. The heatmap is normalized per gene.

In addition to the main auxin, IAA, three other auxins have been described [53]. Of these, only indole-3-butyric acid (IBA) has been clearly shown to be of importance in (root) development [54]. For example, oscillations in IBA production determine pre-branch sites, cells that can potentially form lateral roots at later developmental stages [55,56]. Like IAA, IBA can be conjugated. In addition, it can be converted to IAA and possibly back again [57]. IBA and its conjugates are thereby also a possible storage form of IAA and can influence IAA homeostasis. Conjugation of IBA has been shown to affect salt tolerance because overexpression of UGT74E2, an IBA conjugating enzyme, leads to increased salt tolerance [58]. Whether IBA directly or indirectly – as a storage form of IAA – plays a role remains to be elucidated.

These examples show the importance of including IAA biosynthesis, conjugation, and degradation in the bigger picture of auxin homeostasis and accumulation because these processes may play major roles in the specific regulation of local auxin-mediated responses. However, the wide range of pathways involved in IAA metabolism, the enzymes involved, and their responses to salt stress shows the complexity of interpreting and predicting changes in auxin homeostasis. If we combine this complexity with the observed changes in auxin transport and auxin signaling, predicting the effect of changes in any of these steps can be daunting. More knowledge on the specific regulation of biosynthesis and conjugation enzymes, together with a more comprehensive view of all processes affecting auxin levels and response, will greatly improve our ability to predict the effects of changes in these different components. Incorporation of IAA metabolic pathways into models will also be a great leap forwards for predicting auxin accumulation patterns inside the plant because both processes, in addition to auxin transport, may modulate auxin levels.

Understanding the Role of Auxin in Stress Responses Through Computational Modeling

Predicting the overall role and impact of auxin biosynthesis and short-distance transport compared to long-distance transport in the plant root during development and stress response is a complex task, despite improvements in the sensitivity of *in vivo* auxin reporters [59]. To integrate all components of the different processes that affect local auxin levels, the computational strength of mathematical modeling has proved to be helpful. Many different models concerning auxin or related processes have been created [60].

Although highly instrumental, the current root models have not yet incorporated all relevant parameters and are generally too static to accurately predict the magnitude of the influence of local auxin biosynthesis, conjugation,

and short- and long-distance transport on the root stress response over longer time-periods. Interestingly, recent advances in root modeling show promising results to help to overcome these issues (Box 2). Nonetheless, many valuable insights concerning short-distance auxin transport have come from computational modeling. Until now most computer models have been either analytic one-cell models or describe overall changes in the whole root. Both have been shown to be informative in their own way. For the interplay between auxin and pH, Steinacher *et al.* predict the effect of auxin on intra- and extracellular pH and how this in turn affects auxin concentrations [61]. Their main findings point towards a role for auxin-activated proton pumps which alter proton fluxes, thus affecting auxin transport. By combining the chemiosmotic hypothesis of auxin transport with auxin-induced apoplastic acidification (AAA), they predict increased influx and efflux of auxin, resulting in higher cytosolic auxin concentrations. Another recent single-cell computational model involving lateral root emergence shows the value of computational modeling in local processes involving lateral roots. Mellor *et al.* show that the experimentally observed 'all-or-nothing' _expression pattern of auxin transporter-like protein 3 (LAX3) may be explained by bistability that creates a genetic 'switch' [62]. The model was found to agree with the experimental data only when the exogenously added auxin was decreased over time, suggesting conjugation of auxin and its subsequent degradation. This observation nicely shows the added value of modeling.

An example of the relevance of incorporating auxin conjugation and degradation into auxin computational modeling is a mathematical model describing GH3-mediated auxin conjugation [63]. The model includes the upregulation of GH3 by auxin, thus regulating its own degradation, and positive feedback of auxin on the LAX3 influx carrier. The model predicts oscillation of GH3 and LAX3 mRNA levels after an extracellular auxin increase. In addition, the initial predicted increase of GH3 suggests a possible cellular mechanism to protect cell auxin homeostasis during changes in extracellular auxin levels.

To increase our understanding of long-distance auxin transport, Mitchison *et al.* showed in a single-cell model that combinations of changes in auxin carriers are necessary to mimic experimentally observed auxin flows [64]. Similarly, van den Berg *et al.* and Moore *et al.* have shown in a whole-root model the importance of changes in auxin influx carriers in addition to efflux carriers for modulating auxin flow [9,65].

To date, a model incorporating the changes in auxin biosynthesis and interplay between the different synthesis pathways has yet to be constructed. This follows logically from the fact that much about auxin biosynthesis remains

unknown. However, for a full understanding of changes of auxin in the root during stress the incorporation of realistic changes in auxin synthesis will be necessary.

Nonetheless, multiple studies have now shown model predictions supporting experimental data and have provided suggestions for follow-up experiments. Although *in planta* experiments take significant time in the creation of tools to change single parameters, multiple parameters are easily changed in the models and putative regulators of auxin flow can be found. These regulators can then be verified by in planta experiments. Ideally, a growing and bending model incorporating as many factors as possible – different auxin carriers, hormonal feedback, mechanical feedback, pH changes, and the ability to simulate different stresses – would be useful to make predictions about growth rate and direction during abiotic stress. Furthermore, what modern models are still missing is the ability to show changes in RSA during stress. To elucidate the mechanisms behind different RSA strategies during different abiotic stresses, a model incorporating lateral root emergence and growth through the prediction of the local auxin concentrations is required. Again, such a complex model would need to take into account multiple factors dealing with local auxin maxima around lateral root primordia. Looking to the future of research on complex biological processes, such as the auxin machinery in the plant root, it becomes clear that the field of mathematical modeling will undoubtedly play a key role.

Acknowledgments

This work was supported by ERC Consolidator project Sense2SurviveSalt 724321 and NWO projects ALW 831.15.004 and CW 711.014.002.

Box 1. Apoplastic pH and Auxin Movement

Auxin transport is, in addition to active processes, dependent on passive movement of IAA into or between cells and movement through the apoplast. The concentration of auxin influences apoplastic pH, which in turn influences passive auxin transport into cells. In roots, high cellular auxin concentrations inhibit cell elongation, whereas in the shoot, in accordance with the acid growth theory, auxin causes cell elongation [66,67]. The effect of auxin on apoplastic pH has been demonstrated by the addition of exogenous auxin to arabidopsis roots, which induced fast alkalization of the apoplast [68]. However, after prolonged exposure (8 h) the root apoplast becomes acidified. Similarly, initial alkalization of the apoplast followed by acidification after 19 h was found when endogenous auxin levels were elevated by induced expression of YUCCA6 [68]. Barbez and colleagues have demonstrated that cell-wall acidification triggers cell elongation in arabidopsis seedlings. Their data imply that endogenous auxin concentra-tions regulate apoplast acidification, which in turn regulates cell elongation. During exposure of roots to a salt gradient, auxin redistributes in the root [7,69], suggesting that local alterations in apoplastic pH levels during salt stress might influence cell elongation. In addition, following 1 h root exposure to NaCl a transient increase in apoplastic pH was observed [17]. Following a 100 mM NaCl pulse apoplastic pH returned to control levels 1 h after the transient increase in apoplastic pH. The cytoplasmic pH decreased slightly upon NaCl exposure but did not recover. The changes in passive auxin transport as a result of this alteration in apoplast pH have not yet been studied *in vivo*. Nonetheless, a mathematical/computational model linking auxin and pH dynamics has been created [61]. The main conclusions from this model are that long-term auxin-induced apoplast acidification leads to increased auxin transport across the plasma membrane and significantly higher auxin concentrations in the cytoplasm. However, it has also been reported that the level of passive auxin influx would be negligible at low apoplastic pH (<5.7) in protoplasts [70]. This would mean that all changes in intracellular auxin levels take place through active auxin transport, and there is no role for passive auxin transport in pH-induced alteration of cell elongation during abiotic stress. *In vivo* measurements of cellular auxin influx and efflux during apoplast acidification will be necessary to elucidate the role of passive auxin transport across the plasma membrane.

Box 2. Important Advances in Root Modeling

To create a realistic root model for reliable predictions about changes in auxin flow and local auxin concentrations, several model characteristics need improvement. Two things that will help towards perfecting static 2D models of the root are a realistic root shape and known auxin feedback loops. Van den Berg et al. have shown that both root shape and auxin feedback are important to show experimentally observed changes in auxin flow during halotropism [9]. Another characteristic of the models that needs development is movement. While informative in short-term changes, predictions by static models become less realistic over time because they lack the changes in local auxin maxima that are needed for or caused by growth and bending. Interestingly, recently growing and bending root models have been realized. For example, a model describing a growing and bending root in which local changes in auxin concentrations can be predicted by changing the dynamics of PIN polarization under the influence of changing elastic fields due to root bending was made [71]. Similar to existing experimental data, the auxin concentration was highest at the maximum curvature in the root. Comparable to growing versus static models, the 2D models that are being used now to make predictions of auxin levels are valuable; however, ideally we would want to use a 3D model. Owing to the high complexity, not many 3D root models have been attempted, and those that are available have yet to incorporate many factors. One such 3D model which aims to simulate lateral root emergence through LAX3 and PIN3 modeling has been published [72]. The 3D mathematical model incorporates LAX3 expression and auxin transport. It was found that, for the experimentally observed LAX3 spatial expression to be robust, auxin inducible activity of the PIN3 efflux carrier is required. Consecutive induction of LAX3 and PIN3 ensures stable LAX3 expression.

References

1. Mickelbart, M.V., *et al.* (2015) Genetic mechanisms of abiotic stress tolerance that translate to crop yield stability. *Nat Rev Genet* 16, 237-251.
2. Koevoets, I.T., *et al.* (2016) Roots Withstanding their Environment: Exploiting Root System Architecture Responses to Abiotic Stress to Improve Crop Tolerance. *Front Plant Sci* 7, 1335.
3. Di Mambro, R., *et al.* (2017) Auxin minimum triggers the developmental switch from cell division to cell differentiation in the Arabidopsis root. *Proc Natl Acad Sci U S A* 114, E7641-E7649.
4. Adamowski, M., *et al.* (2015) PIN-dependent auxin transport: action, regulation, and evolution. *Plant Cell* 27, 20-32.
5. Naramoto, S. (2017) Polar transport in plants mediated by membrane transporters: focus on mechanisms of polar auxin transport. *Curr Opin Plant Biol* 40, 8-14.
6. Armengot, L., *et al.* (2016) Regulation of polar auxin transport by protein and lipid kinases. *J Exp Bot* 67, 4015-4037.
7. Galvan-Ampudia, C.S., *et al.* (2013) Halotropism is a response of plant roots to avoid a saline environment. *Curr Biol* 23, 2044-2050.
8. Zwiewka, M., *et al.* (2015) Osmotic Stress Modulates the Balance between Exocytosis and Clathrin-Mediated Endocytosis in Arabidopsis thaliana. *Mol Plant* 8, 1175-1187.
9. van den Berg, T., *et al.* (2016) Modeling halotropism: a key role for root tip architecture and reflux loop remodeling in redistributing auxin. *Development* 143, 3350-3362.
10. Liu, W., *et al.* (2015) Salt stress reduces root meristem size by nitric oxide-mediated modulation of auxin accumulation and signaling in Arabidopsis. *Plant Physiol* 168, 343-356.
11. Geisler, M., *et al.* (2017) A Critical View on ABC Transporters and Their Interacting Partners in Auxin Transport. *Plant Cell Physiol* 58, 1601-1614.
12. Chai, C., *et al.* (2016) Comprehensive Analysis and Expression Profiling of the OsLAX and OsABCB Auxin Transporter Gene Families in Rice (Oryza sativa) under Phytohormone Stimuli and Abiotic Stresses. *Front Plant Sci* 7, 593.
13. Han, E.H., *et al.* (2017) 'Bending' models of halotropism: incorporating protein phosphatase 2A, ABCB transporters, and auxin metabolism. *J Exp Bot.* 68, 3071-3089.
14. Cho, M., *et al.* (2014) Block of ATP-binding cassette B19 ion channel activity by 5-nitro-2-(3-phenylpropylamino)-benzoic acid impairs polar auxin transport and root gravitropism. *Plant Physiol* 166, 2091-2099.
15. Dalal, J., *et al.* (2016) ROSY1, a novel regulator of gravitropic response is a stigmasterol binding protein. *J Plant Physiol* 196-197, 28-40.

16. Remy, E.*, et al.* (2013) A major facilitator superfamily transporter plays a dual role in polar auxin transport and drought stress tolerance in Arabidopsis. *Plant Cell* 25, 901-926.
17. Gao, D.*, et al.* (2004) Self-reporting Arabidopsis expressing pH and [Ca2+] indicators unveil ion dynamics in the cytoplasm and in the apoplast under abiotic stress. *Plant Physiol* 134, 898-908.
18. Ranocha, P.*, et al.* (2013) Arabidopsis WAT1 is a vacuolar auxin transport facilitator required for auxin homoeostasis. *Nat Commun* 4, 2625.
19. Barbez, E.*, et al.* (2012) A novel putative auxin carrier family regulates intracellular auxin homeostasis in plants. *Nature* 485, 119-122.
20. Han, X.*, et al.* (2014) Auxin-callose-mediated plasmodesmal gating is essential for tropic auxin gradient formation and signaling. *Dev Cell* 28, 132-146.
21. Di, D.-W.*, et al.* (2015) The biosynthesis of auxin: how many paths truly lead to IAA? *Plant Growth Regulation* 78, 275-285.
22. Tivendale, N.D.*, et al.* (2014) The shifting paradigms of auxin biosynthesis. *Trends Plant Sci* 19, 44-51.
23. Mashiguchi, K., Tanaka, K., Sakai, T., Sugawara, S., Kawaide, H., Natsume, M., ... & McSteen, P. (2011) The main auxin biosynthesis pathway in Arabidopsis. *Proc Natl Acad Sci U S A* 108, 18512-18517.
24. Won, C., Shen, X., Mashiguchi, K., Zheng, Z., Dai, X., Cheng, Y., ... & Zhao, Y. (2011) Conversion of tryptophan to indole-3-acetic acid by TRYPTOPHAN AMINOTRANSFERASES OF ARABIDOPSIS and YUCCAs in Arabidopsis. *Proc Natl Acad Sci U S A* 108, 18518-18523.
25. Julkowska, M.M.*, et al.* (2017) Genetic Components of Root Architecture Remodeling in Response to Salt Stress. *Plant Cell* 29, 3198-3213.
26. Lehmann, T.*, et al.* (2017) Arabidopsis NITRILASE 1 Contributes to the Regulation of Root Growth and Development through Modulation of Auxin Biosynthesis in Seedlings. *Front Plant Sci* 8, 36.
27. Zhao, Y., Hull, A. K., Gupta, N. R., Goss, K. A., Alonso, J., Ecker, J. R., ... & Celenza, J. L. (2002) Trp-dependent auxin biosynthesis in Arabidopsis: involvement of cytochrome P450s CYP79B2 and CYP79B3. *Genome Res* 16, 3100-3112.
28. Stepanova, A.N.*, et al.* (2008) TAA1-mediated auxin biosynthesis is essential for hormone crosstalk and plant development. *Cell* 133, 177-191.
29. Tao, Y.*, et al.* (2008) Rapid synthesis of auxin via a new tryptophan-dependent pathway is required for shade avoidance in plants. *Cell* 133, 164-176.
30. Chen, Q.*, et al.* (2014) Auxin overproduction in shoots cannot rescue auxin deficiencies in Arabidopsis roots. *Plant Cell Physiol* 55, 1072-1079.

31. Cheng, Y., *et al.* (2006) Auxin biosynthesis by the YUCCA flavin monooxygenases controls the formation of floral organs and vascular tissues in Arabidopsis. *Genes Dev* 20, 1790-1799.
32. Li, L., *et al.* (2012) Linking photoreceptor excitation to changes in plant architecture. *Genes Dev* 26, 785-790.
33. Nozue, K., *et al.* (2015) Shade avoidance components and pathways in adult plants revealed by phenotypic profiling. *PLoS Genet* 11, e1004953.
34. Ke, Q., *et al.* (2015) Transgenic poplar expressing Arabidopsis YUCCA6 exhibits auxin-overproduction phenotypes and increased tolerance to abiotic stress. *Plant Physiol Biochem* 94, 19-27.
35. Kim, J.I., *et al.* (2013) Overexpression of Arabidopsis YUCCA6 in potato results in high-auxin developmental phenotypes and enhanced resistance to water deficit. *Mol Plant* 6, 337-349.
36. Yan, S., *et al.* (2016) Different cucumber CsYUC genes regulate response to abiotic stresses and flower development. *Sci Rep* 6, 20760.
37. Dinneny, J.R., *et al.* (2008) Cell Identity Mediates the Response of Arabidopsis Roots to Abiotic Stress. *Science* 320, 942-945.
38. Kilian, J., *et al.* (2007) The AtGenExpress global stress expression data set: protocols, evaluation and model data analysis of UV-B light, drought and cold stress responses. *Plant J* 50, 347-363.
39. Glawischnig, E., Hansen, B. G., Olsen, C. E., & Halkier, B. A. (2004) Camalexin is synthesized from indole-3-acetaldoxime, a key branching point between primary and secondary metabolism in Arabidopsis. *Proc Natl Acad Sci U S A* 101, 8245-8250.
40. Hull, A.K., *et al.* (1999) Arabidopsis cytochrome P450s that catalyze the first step of tryptophan-dependent indole-3-acetic acid biosynthesis. *Proc Natl Acad Sci U S A* 97, 2379–2384.
41. Mikkelsen, M.D., *et al.* (2000) Cytochrome P450 CYP79B2 from Arabidopsis catalyzes the conversion of tryptophan to indole-3-acetaldoxime, a precursor of indole glucosinolates and indole-3-acetic acid. *J Biol Chem* 275, 33712-33717.
42. Sugawara, S., *et al.* (2009) Biochemical analyses of indole-3-cetaldoximedependent auxin biosynthesis in Arabidopsis. *Proc Natl Acad Sci U S A* 106, 5430-5435.
43. Ljung, K., *et al.* (2005) Sites and regulation of auxin biosynthesis in Arabidopsis roots. *Plant Cell* 17, 1090-1104.
44. Ludwig-Muller, J. (2011) Auxin conjugates: their role for plant development and in the evolution of land plants. *J Exp Bot* 62, 1757-1773.
45. Kowalczyk, M., *et al.* (2001) Quantitative Analysis of Indole-3-Acetic Acid Metabolites in Arabidopsis. *Plant Physiology* 127, 1845-1853.
46. Östin, A., Kowalyczk, M., Bhalerao, R.P., and Sandberg, G. (1998) Metabolism of Indole-3-Acetic Acid in Arabidopsis. *Plant Physiol* 118, 285-296.

47. Mellor, N., *et al.* (2016a) Dynamic regulation of auxin oxidase and conjugating enzymes AtDAO1 and GH3 modulates auxin homeostasis. *Proc Natl Acad Sci U S A* 113, 11022-11027.
48. Staswick, P.E., *et al.* (2005) Characterization of an Arabidopsis enzyme family that conjugates amino acids to indole-3-acetic acid. *Plant Cell* 17, 616-627.
49. Park, J.E., *et al.* (2007) GH3-mediated auxin homeostasis links growth regulation with stress adaptation response in Arabidopsis. *J Biol Chem* 282, 10036-10046.
50. Zhang, J., *et al.* (2017) Auxin homeostasis: the DAO of catabolism. *J Exp Bot* 68, 3145-3154.
51. Porco, S., *et al.* (2016) Dioxygenase-encoding AtDAO1 gene controls IAA oxidation and homeostasis in Arabidopsis. *Proc Natl Acad Sci U S A* 113, 11016-11021.
52. Zhang, J., *et al.* (2016) DAO1 catalyzes temporal and tissue-specific oxidative inactivation of auxin in Arabidopsis thaliana. *Proc Natl Acad Sci U S A* 113, 11010-11015.
53. Simon, S., *et al.* (2011) Why plants need more than one type of auxin. *Plant Sci* 180, 454-460.
54. Frick, E.M., *et al.* (2018) Roles for IBA-derived auxin in plant development. *J Exp Bot* 69, 169-177.
55. De Rybel, B., *et al.* (2012) A role for the root cap in root branching revealed by the non-auxin probe naxillin. *Nat Chem Biol* 8, 798-805.
56. Xuan, W., *et al.* (2015) Root Cap-Derived Auxin Pre-patterns the Longitudinal Axis of the Arabidopsis Root. *Curr Biol* 25, 1381-1388.
57. Liu, X., *et al.* (2012) Transport of indole-3-butyric acid and indole-3-acetic acid in Arabidopsis hypocotyls using stable isotope labeling. *Plant Physiol* 158, 1988-2000.
58. Tognetti, V.B., *et al.* (2010) Perturbation of indole-3-butyric acid homeostasis by the UDP-glucosyltransferase UGT74E2 modulates Arabidopsis architecture and water stress tolerance. *Plant Cell* 22, 2660-2679.
59. Liao, C.Y., *et al.* (2015) Reporters for sensitive and quantitative measurement of auxin response. *Nat Methods* 12, 207-210, 202 p following 210.
60. Morales-Tapia, A., *et al.* (2016) Computational Modeling of Auxin: A Foundation for Plant Engineering. *Front Plant Sci* 7, 1881.
61. Steinacher, A., *et al.* (2012) A computational model of auxin and pH dynamics in a single plant cell. *J Theor Biol* 296, 84-94.
62. Mellor, N., *et al.* (2015) Modelling of Arabidopsis LAX3 expression suggests auxin homeostasis. *J Theor Biol* 366, 57-70.
63. Mellor, N., *et al.* (2016b) GH3-Mediated Auxin Conjugation Can Result in Either Transient or Oscillatory Transcriptional Auxin Responses. *Bull Math Biol* 78, 210-234.

64. Mitchison, G. (2015) The Shape of an Auxin Pulse, and What It Tells Us about the Transport Mechanism. *PLoS Comput Biol* 11, e1004487.
65. Moore, S.*, et al.* (2017) A recovery principle provides insight into auxin pattern control in the Arabidopsis root. *Sci Rep* 7, 43004.
66. Rayle, D.L.a.C., R. (1970) Enhancement of Wall Loosening and Elongation by Acid Solutions. *Plant Physiol* 46, 250-253.
67. Rayle, D.L.a.C., R. E. (1992) The Acid Growth Theory of Auxin-Induced Cell Elongation Is Alive and Well. *Plant Physiol* 99, 1271-1274.
68. Barbez, E.*, et al.* (2017) Auxin steers root cell expansion via apoplastic pH regulation in Arabidopsis thaliana. *Proc Natl Acad Sci U S A* 114, E4884-E4893.
69. Wang, Y.*, et al.* (2009) Auxin redistribution modulates plastic development of root system architecture under salt stress in Arabidopsis thaliana. *J Plant Physiol* 166, 1637-1645.
70. Rutschow, H.L.*, et al.* (2014) The carrier AUXIN RESISTANT (AUX1) dominates auxin flux into Arabidopsis protoplasts. *New Phytol* 204, 536-544.
71. Romero-Arias, J.R.*, et al.* (2017) Model of polar auxin transport coupled to mechanical forces retrieves robust morphogenesis along the Arabidopsis root. *Phys Rev E* 95, 032410.
72. Peret, B.*, et al.* (2013) Sequential induction of auxin efflux and influx carriers regulates lateral root emergence. *Mol Syst Biol* 9, 699.
73. Peret, B. (2017) Primary and lateral root.ai. figshare.

Supplemental table 1. Micro-array data in control and salt stress published previously (Dinneny et al. 2008, Killian et al. 2007) for genes described to be involved in either biosynthesis or conjugation of IAA. The data has been derived from the EfP browser website and the normalisation as published on this website has been used. Zones and tissues are illustrated in figure 2A. Relative values represent log2 fold change of expression upon salt stress.

Enzyme	Gene	Substrate	Product	Shoot_C	Shoot_S1hr	Root_C	Root_S1hr	0hr_MS	30min_NaCl	1hr_NaCl	4hr_NaCl	16hr_NaCl	32hr_NaCl	ZONE1_STAI	ZONE2_STAI	ZONE3_STAI	ZONE4_STAI	ZONE1_NAC	ZONE2_NAC	ZONE3_NAC
1a IpyA pathway																				
*Tryptophan Aminotransferase of Arabidopsis **Tryptophan Aminotransferase Related ***YUCCA flavin monooxygenase																				
TAA1*	AT1G70560	Tryptophan	Indole-3-pyruvic Acid	55.8	89.69	82.07	92.66	89.17	102.89	146.01	170.83	102.22	92.76	108.25	249.78	202.08	12.32	149.04	478.72	410.28
TAR1**	AT1G23320	Tryptophan	Indole-3-pyruvic Acid	4.09	1.24	3.04	0.66	1.13	3.24	2.34	1.38	2.3	2.78	6.76	2.91	5.32	1.37	5.75	9.03	6.15
TAR2**	AT4G24670	Tryptophan	Indole-3-pyruvic Acid	80.19	73.52	46.13	22.57	20.12	22.37	9.28	5.48	4.46	5.44	10.45	4.95	17.04	16.55	12.68	0.78	13.95
TAR3**	AT1G34040	Tryptophan	Indole-3-pyruvic Acid	8.71	13.41	77.84	56.88	133.45	105	101.59	66.47	121.23	137.09	4.35	2.95	61.48	270.25	11.79	8.58	59.23
TAR4**	AT1G34060	Tryptophan	Indole-3-pyruvic Acid	8.71	13.41	77.84	56.88	133.45	105	101.59	66.47	121.23	137.09	4.35	2.95	61.48	270.25	11.79	8.58	59.23
YUC1***	AT4G32540	Indole-3-pyruvic Acid	Indole-3-acetic Acid	15.43	16.5	11.21	12.59	6.69	7.16	10.38	7.71	3.29	6.1	20.46	19.61	21.89	13.55	19.51	22.33	19.02
YUC2***	AT4G13260	Indole-3-pyruvic Acid	Indole-3-acetic Acid	79.24	84.18	28.46	33.08	11.63	11.58	14.93	20.28	15.86	14.88	32.31	32.71	27.28	23.16	44.25	36.5	33.95
YUC3***	AT1G04610	Indole-3-pyruvic Acid	Indole-3-acetic Acid	21.05	28.75	103.69	129.78	39.17	32.96	41.36	38.83	30.46	27.02	440.41	40.86	164.04	18.67	702.47	37.83	67.94
YUC4***	AT5G11320	Indole-3-pyruvic Acid	Indole-3-acetic Acid	9.51	8.6	2.07	9.11	0.94	2	2.11	3.46	2.17	1.69	7.4	8.18	10.55	9.01	11	2.6	8.88
YUC5***	At5g43890	Indole-3-pyruvic Acid	Indole-3-acetic Acid	8.82	6.56	14.61	33.85	19.31	55.98	37.27	35.73	29	21.49	8.78	9.02	98.69	60.8	11.31	45.84	107.59
YUC6***	At5g25620	Indole-3-pyruvic Acid	Indole-3-acetic Acid	4.21	3.08	21.3	15.37	4.53	5.57	5.27	7.71	4.41	3.59	2.43	1.48	2.54	11.71	2.76	1.79	5.23
YUC7***	At2g33230	Indole-3-pyruvic Acid	Indole-3-acetic Acid	5.8	1.99	4.47	4.01	6.71	5.26	2.13	6.39	3.48	5.52	23.45	1.79	9.12	4.46	35.11	2.57	6.24
YUC8***	At4g28720	Indole-3-pyruvic Acid	Indole-3-acetic Acid	13.7	21.23	56.25	61.46	11.95	19.63	13.52	21.53	13.34	11.82	50.09	10.67	36.63	17.77	73.92	12.05	21.15
YUC9***	at1g04180	Indole-3-pyruvic Acid	Indole-3-acetic Acid	1.58	2.1	22.09	35.12	11.46	35.2	42.19	30.64	12.18	17.62	64	9.65	40.75	20.28	72.94	87.34	100.49
YUC10***	At1g48910	Indole-3-pyruvic Acid	Indole-3-acetic Acid	18.58	23.21	11.4	8.29	3.4	1.68	3.78	6.49	3.54	3.12	9.36	10.83	6.95	10.87	16.17	2.46	7.22
YUC11***	At1g21430	Indole-3-pyruvic Acid	Indole-3-acetic Acid	1.04	1.54	5.21	2.99	4.43	1.75	4.52	2.71	1.67	1.37	11.46	5.67	1.92	1.33	10.34	3.13	5.08
1b IAOx pathway																				
*Cytochrome P450 **Nitrilase																				
CYP79B2*	AT4G39950	Tryptophan	Indole-3-acetaldoxime	100.13	86.12	909.9	795.25	198.28	237.46	130.9	73.86	324.71	300.87	408.84	16.05	110.41	735.11	69.74	10.84	125.25
CYP79B3*	AT2G22330	Tryptophan	Indole-3-acetaldoxime	72.18	81.72	747.84	545.36	109.94	110.17	54.97	20.07	90.01	56.24	66.5	7.19	24.8	289.69	33.34	12.71	23.94
NIT1**	AT3G44310	Indole-3-acetonitrile	Indole-3-acetic Acid	2468.29	2350.38	665.43	813.47	1164.09	1334.71	1276.08	1139.37	1125.99	1575.71	176.57	525.96	408.76	1429.68	223.97	601.95	656.5
NIT2**	AT3G44300	Indole-3-acetonitrile	Indole-3-acetic Acid	2468.29	2350.38	665.43	813.47	1164.09	1334.71	1276.08	1139.37	1125.99	1575.71	176.57	525.96	408.76	1429.68	223.97	601.95	656.5
NIT3**	AT3G44320	Indole-3-acetonitrile	Indole-3-acetic Acid	45.14	34.08	175.95	167.05	510.17	499.81	526.75	548.38	505.27	488.04	188.96	444.61	163.44	1002.1	138.07	438.55	146.12
2a Ester conjugation																				
*UDP-glucose transferase																				
IAGLU*	AT4G15550	Indole-3-acetic Acid	1-O-indole-3-acetyl-b-D-glucose	158.35	141.47	144.98	169.19	571.8	449.03	435.81	561.37	472.49	652.65	912.71	486.37	295.86	757.98	1168.54	632.15	973.97
UGT84B1*	At2G23260	Indole-3-acetic Acid	1-O-indole-3-acetyl-b-D-glucose	0.96	2.99	1.05	1.9	0.57	0.55	0.48	1.27	3.18	1.07	1.1	0.57	1.75	2.04	1.17	1.15	2.5
UGT84B2*	At2G23250	Indole-3-acetic Acid	1-O-indole-3-acetyl-b-D-glucose	1.46	1.63	1.52	4.07	2.61	0.46	0.91	0.95	2.84	0.78	2.9	0.61	4.54	1.44	2.46	0.85	7.14
UGT75B1*	AT1G05560	Indole-3-acetic Acid	1-O-indole-3-acetyl-b-D-glucose	140.86	53.39	39.71	73.89	170.17	326.14	368.71	235.05	95.11	104.48	68.51	180.96	314.17	252.76	179.81	498.1	657.83
UGT75B2*	AT1G05530	Indole-3-acetic Acid	1-O-indole-3-acetyl-b-D-glucose	6.32	5.5	15.32	11.97	21.53	39.33	37.94	34.08	31.53	33.75	24.75	63.59	50.84	2.56	21.73	149.2	39.6
2b Amide conjugation																				
*GRETCHEN HAGEN 3 family protein **There are several amino-acid conjugations possible																				
GH3.2*	AT4G37390	Indole-3-acetic Acid	Indole-3-acetyl-amide**	1.61	1.33	184.33	840.64	3.46	1.13	4.32	115.75	2	NA	3.46	1.13	4.32	115.75	0.55	0.94	59.49
GH3.3*	AT2G23170	Indole-3-acetic Acid	Indole-3-acetyl-amide**	52.49	43.37	168.08	1834.48	241.15	401.25	387.24	38.03	120.76	27.22	1.58	0.59	2.54	242.94	1.33	3.38	17.84
GH3.4*	AT1G59500	Indole-3-acetic Acid	Indole-3-acetyl-amide**	1.61	1.33	184.33	840.64	22.93	15.28	24.42	10.51	15.39	6.65	3.46	1.13	4.32	115.75	0.55	0.94	59.49
GH3.5/WES1	AT4G27260	Indole-3-acetic Acid	Indole-3-acetyl-amide**	44.34	73.09	156.13	279.97	40.28	28.68	24.27	29.17	24.97	19.54	66.33	16.59	28.27	52.33	35.01	20.76	50.9
GH3.6*	AT5G54510	Indole-3-acetic Acid	Indole-3-acetyl-amide**	107.61	171.19	139.94	230.61	2.99	2.98	3.03	3.57	2.79	2.66	105.19	17.21	22.11	178.23	30.04	23.4	42.34
GH3.17*	AT1G28130	Indole-3-acetic Acid	Indole-3-acetyl-amide**	23.09	30.15	398.13	427.47	99.76	63.96	58.27	146.14	100.5	172.93	180.24	63.44	71.42	51.85	50.25	54.32	69.47
2c Oxidation																				
*Dioxygenase for auxin oxidation																				
DAO1*	AT1G14130	Indole-3-acetic Acid	2-oxindole-3-acetic acid	43.73	45.64	77.8	114.69	89.05	110.21	104.18	59.4	91.09	97.05	24.67	37.76	35.34	179.47	47.67	37.71	30.72
DAO2*	AT1G14120	Indole-3-acetic Acid	2-oxindole-3-acetic acid	25.53	14.21	163.28	185.19	75.56	71.4	45.8	33.67	49.06	49.7	2.69	4.9	2.32	176.32	0.5	0.42	3.26

ZONE4_NAC	Zone1_rel	Zone2_rel	Zone3_rel	Zone4_rel	EPI_STANDA	COL_STAND/	COR_STAND	END_STAND	STE_STAND/	PHI_STAND/	EPI_NACL	COL_NACL	COR_NACL	END_NACL	STE_NACL	PHI_NACL	EPI_rel	COL_rel	COR_rel	END_rel	STE_rel	PHI_rel
28.75	0.46	0.94	1.02	1.22	127.8	200.7	20.68	55.99	330.72	57.26	410.32	146	133.31	132.34	303.5	174.92	1.68286164	-0.4590722	2.68847692	1.2410081	-0.1239138	1.61109568
3.02	-0.23	1.63	0.21	1.14	1.71	1.88	1.5	2.28	7.66	6.43	3.48	0.62	7.61	2.75	2.89	3.56	1.02509098	-1.6003925	2.34293395	0.27039779	-1.4062749	-0.8529415
9.5	0.28	-2.67	-0.29	-0.8	15.07	50.16	0.58	7.95	12.66	197.34	44.18	11.94	9.19	1.5	14.92	142.41	1.551714	-2.0707345	3.98594006	-2.4059924	0.23697013	-0.470633
192.48	1.44	1.54	-0.05	-0.49	19.11	24.26	135.5	156.91	41.83	13.9	25.73	19.8	140.99	128.83	21.92	7.54	0.42912368	-0.2930791	0.05729999	-0.2844687	-0.9322902	-0.8824485
192.48	1.44	1.54	-0.05	-0.49	19.11	24.26	135.5	156.91	41.83	13.9	25.73	19.8	140.99	128.83	21.92	7.54	0.42912368	-0.2930791	0.05729999	-0.2844687	-0.9322902	-0.8824485
15.32	-0.07	0.19	-0.2	0.18	10.95	18.11	12.57	12.74	17.55	36.61	13.79	16.73	26.08	10.45	8.2	10.76	0.33269159	-0.1143491	1.05295922	-0.2858623	-1.0977752	-1.7665597
24.8	0.45	0.16	0.32	0.1	21.28	40.13	30.35	31.4	32.11	42.02	23.01	25.71	43.48	20.5	29.37	31.56	0.11276283	-0.6423515	0.51865542	-0.6151406	-0.1286794	-0.412979
25.05	0.67	-0.11	-1.27	0.42	191.89	2932.11	48.92	138.73	113.44	62.51	747.11	2411.1	162.98	384.61	104.06	90.76	1.96104114	-0.2822477	1.73619863	1.47111647	-0.1245138	0.53796961
4.23	0.57	-1.65	-0.25	-1.09	4.77	17.51	7.03	12.72	9.93	9.09	6.26	8.89	16.38	12.33	6.79	12.91	0.39217339	-0.9779238	1.22033876	-0.0449259	-0.5483821	0.5061368
79.62	0.37	2.35	0.12	0.39	19.51	271.89	13.8	193.21	206.51	808.97	332.18	272.33	125.72	134.83	461.27	683.29	4.08967953	0.00233283	3.18747401	-0.5190282	1.15939982	-0.2435882
14.44	0.18	0.27	1.04	0.3	3.67	3.98	3.09	3.21	4.03	21.27	2.31	4.51	5.23	1.71	3.75	3.62	-0.6678872	0.180359	0.75920411	-0.908577	-0.1038892	-2.5547584
2.37	0.58	0.52	-0.55	-0.91	2.01	306.27	2.89	5.41	6.01	3.94	2.93	214.23	8.49	3.42	0.97	1.21	0.54370516	-0.5156435	1.55469506	-0.6616323	-2.6313083	-1.7031886
5.86	0.56	0.18	-0.79	-1.6	107.79	1335.85	11.24	52.29	115.17	62.79	306.15	1365.36	78.32	75.85	87.75	58.81	1.50601534	0.03152337	2.80073873	0.53661411	-0.3922939	-0.0944733
15.53	0.19	3.18	1.3	-0.38	68.82	1135.49	14.85	22.93	36.01	85.37	473.37	817.76	46.64	29.7	51.99	43.12	2.78206848	-0.4735656	1.65110486	0.37322658	0.52983656	-0.985372
12.02	0.79	-2.14	0.05	0.15	2.25	15.93	5.73	8.75	11.83	31.63	8.04	14.03	22.32	14.51	8.76	14.43	1.8372705	-0.1832313	1.96172998	0.7296926	-0.4334473	-1.1322223
5.5	-0.15	-0.86	1.4	2.05	1.57	5.47	0.89	5.83	5.51	4.96	0.81	2.45	5.2	5.62	2.96	1.7	-0.9547707	-1.1587591	2.54663438	-0.0529258	-0.8964551	-1.5448054
364.49	-2.55	-0.57	0.18	-1.01	107.08	279.53	83.37	382.78	161.56	696.48	146.18	137.38	76.53	191.87	96.61	309.58	0.4490569	-1.0248311	-0.1235029	-0.9963863	-0.7418256	-1.1697697
189.39	-1	0.82	-0.05	-0.61	12.36	53.28	34.48	122.91	82.6	213.77	11.36	13.82	58.85	71.81	50.16	81.93	-0.1217159	-1.9468365	0.77128264	-0.7753456	-0.7196044	-1.3835957
1343.88	0.34	0.19	0.68	-0.09	407.17	112.95	1551.4	451.66	303.67	89.46	252.72	61.15	1469.42	400.32	306.23	114.42	-0.6880914	-0.8852599	-0.0783239	-0.1740835	0.01211124	0.35502459
1343.88	0.34	0.19	0.68	-0.09	407.17	112.95	1551.4	451.66	303.67	89.46	252.72	61.15	1469.42	400.32	306.23	114.42	-0.6880914	-0.8852599	-0.0783239	-0.1740835	0.01211124	0.35502459
795.17	-0.45	-0.02	-0.16	-0.33	403.21	478.84	1411.46	604.83	156.06	72.66	542.63	387.57	1204	472.11	112.1	69.37	0.42843739	-0.3050868	-0.2293529	-0.3574067	-0.4773145	-0.0668495
453.82	0.36	0.38	1.72	-0.74	292.79	386.34	257.06	552.59	116.54	66.68	878.09	1189.89	299.38	898.78	197.35	117.87	1.58450254	1.62288525	0.21987271	0.70175857	0.7599313	0.82187056
2	0.09	1.01	0.51	-0.03	0.79	2.69	2.2	2.01	3.61	10.27	0.85	1.23	1.39	1.36	0.79	1.94	0.10561019	-1.1289479	-0.6624186	-0.5635889	-2.1920743	-2.4043076
1.36	-0.24	0.48	0.65	-0.08	2.58	5.25	2.91	1.05	8.78	7.07	2.36	1.56	9.07	1.49	1.68	1.26	-0.1285842	-1.7507714	1.6400834	0.504923	-2.3857597	-2.4882865
424.09	1.39	1.46	1.07	0.75	76.31	9.68	103.76	31.31	10.09	8.15	783.47	48.96	128.54	91.82	151.01	37.86	3.359934	2.33852461	0.30896699	1.55218492	3.90364601	2.21580245
4.39	-0.19	1.23	-0.36	0.78	72.79	10.54	8.8	5.79	13.38	1.19	169.27	25.83	25.03	6.28	22.95	19.86	1.21751414	1.29317278	1.50808286	0.11720121	0.77841604	4.06083214
67.52	-2.65	-0.27	3.78	-0.78	36.94	258.92	108.2	210.99	77.03	11.59	211.53	140.61	145.59	684.95	131.72	20.04	2.51760652	-0.8808072	0.42821077	1.69882406	0.77398209	0.79000194
55.96	-0.25	2.52	2.81	-2.12	3.29	20.59	629.31	131.58	36.72	14.95	72.78	15.34	378.94	253.51	139.21	69.58	4.46738256	-0.4246453	-0.7318014	0.94610244	1.92262489	2.2185272
67.52	-2.65	-0.27	3.78	-0.78	36.94	258.92	108.2	210.99	77.03	11.59	211.53	140.61	145.59	684.95	131.72	20.04	2.51760652	-0.8808072	0.42821077	1.69882406	0.77398209	0.79000194
42.13	-0.92	0.32	0.85	-0.31	43.51	349.27	63.56	124.72	120.85	83.39	58.24	69.42	111.84	178.61	184.48	83.94	0.42066334	-2.3309195	0.81524524	0.51812002	0.61024695	0.00948408
342.99	-1.81	0.44	0.94	0.94	72.24	919.1	282.53	127.79	165.43	69.64	214.58	500.43	1008.06	151.66	200.3	63.14	1.57064582	-0.8770536	1.83510554	0.24706568	0.27594154	-0.1413619
158.87	-1.84	-0.22	-0.04	1.62	310.44	1471.57	389.41	48.6	46.2	12.22	187.05	133.18	788.34	86.14	38.28	16.3	-0.7308905	-3.4659068	1.01752805	0.82572701	-0.271302	0.41562768
83.57	0.95	0	-0.2	-1.1	28.32	81.98	175.96	86.07	34.17	59.58	51.87	166.42	41.66	50.11	50.99	102.7	0.8730791	1.02148493	-2.0785128	-0.7804119	0.57748409	0.78553615
66.8	-2.43	-3.54	0.49	-1.4	0.19	3.28	22.98	3.87	3.04	4.54	1.57	0.46	13.23	3.5	0.67	0.44	3.04669324	-2.83399	-0.7965657	-0.1449786	-2.1818383	-3.3671169